Journal of Geophysical Research: Earth Surface

RESEARCH ARTICLE
10.1029/2017JF004597

Drivers of Firn Density on the Greenland Ice Sheet Revealed by Weather Station Observations and Modeling

B. Vandecrux[1,2], R. S. Fausto[1], P. L. Langen[3], D. van As[1], M. MacFerrin[4], W. T. Colgan[1], T. Ingeman-Nielsen[2], K. Steffen[5], N. S. Jensen[6], M. T. Møller[6], and J. E. Box[1]

[1]Geological Survey of Denmark and Greenland, Copenhagen, Denmark, [2]Department of Civil Engineering, Technical University of Denmark, Kgs. Lyngby, Denmark, [3]Climate and Arctic Research, Danish Meteorological Institute, Copenhagen, Denmark, [4]Cooperative Institute for Research in Environmental Sciences, University of Colorado Boulder, Boulder, CO, USA, [5]Swiss Federal Institute for Forest, Snow, and Landscape Research (WSL), Birmensdorf, Switzerland, [6]Department of Environmental Engineering, Technical University of Denmark, Kgs. Lyngby, Denmark

Abstract Recent Arctic atmospheric warming induces more frequent surface melt in the accumulation area of the Greenland ice sheet. This increased melting modifies the near-surface firn structure and density and may reduce the firn's capacity to retain meltwater. Yet few long-term observational records are available to determine the evolution and drivers of firn density. In this study, we compile and gap-fill Greenland Climate Network (GC-Net) automatic weather station data from Crawford Point, Dye-2, NASA-SE, and Summit between 1998 and 2015. These records then force a coupled surface energy balance and firn evolution model. We find at all sites except Summit that increasing summer turbulent heat fluxes to the surface are compensated by decreasing net radiative fluxes. After evaluating the model against firn cores, we find that, starting from 2006, the density of the top 20 m of firn at Dye-2 increased by 11%, decreasing the pore volume by 18%. Crawford Point and Summit show stable near-surface firn density over 1998–2010 and 2000–2015 respectively, while we calculate a 4% decrease of firn density at NASA-SE over 1998–2015. For each year, the model identifies the drivers of density change in the top 20-m firn and quantifies their contributions. The key driver, snowfall, explains alone 72 to 92% of the variance in day-to-day change in firn density while melt explains from 7 to 33%. Our result indicates that correct estimates of the magnitude and variability of precipitation are necessary to interpret or simulate the evolution of the firn.

Plain Language Summary Arctic warming has led to more intense melt on the Greenland ice sheet. In recent decades this melt moved upglacier and started to alter the structure of perennial snow, or firn, in areas where melt was rarely recorded. In this study, we process 12–17 years of observations from four weather stations located in the vast high-elevation area of the ice sheet. From these climate records, we calculate how much melt occurred each summer and why (e.g., warm air or sunlight absorption). We found that heat transfer from the air to the surface has become more intense but is compensated by a brightening of the surface, causing less sunlight to be absorbed and used for melting. We use a computer model that simulates firn evolution and shows a good match with independent observations of the firn density. Our simulations identify increasing firn density at a first site, stable density at two sites, and decreasing firn density at the last one. Day-to-day and year-to-year changes in the density of the top 20 m of firn were mostly due to the snowfall variability followed by surface melt. This work underlines the importance of accurate precipitation estimates in order to understand firn evolution.

Key Points:
- We gathered, processed, and gap-filled underexploited climate observations at four sites from the Greenland ice sheet accumulation area
- Increasing turbulent heat fluxes were found at three sites over the 1998–2015 period, compensated by decreasing net radiative fluxes
- Our simulation of near-surface firn density quantifies the role of its climatic drivers among which snowfall and surface melt are dominant

Supporting Information:
- Supporting Information S1

Correspondence to:
B. Vandecrux,
bava@byg.dtu.dk

Citation:
Vandecrux, B., Fausto, R. S., Langen, P. L., van As, D., MacFerrin, M., Colgan, W. T., et al. (2018). Drivers of firn density on the Greenland ice sheet revealed by weather station observations and modeling. *Journal of Geophysical Research: Earth Surface*, *123*, 2563–2576. https://doi.org/10.1029/2017JF004597

Received 27 DEC 2017
Accepted 23 SEP 2018
Accepted article online 27 SEP 2018
Published online 24 OCT 2018

1. Introduction

Over the past two decades, the Greenland ice sheet has experienced significant atmospheric warming (e.g., Box, 2013; Hanna et al., 2008). As a result, the ice sheet loses mass at an increasing rate (e.g., Khan et al., 2015; van den Broeke et al., 2016) due to increasing meltwater runoff and accelerated ice flow discharge to the sea (e.g., Enderlin et al., 2014). Surface melt is common at the ice sheet margin, but has reached high elevations in the past decade (Fettweis et al., 2011; Nghiem et al., 2012; Tedesco et al., 2011). Beyond increasing air temperatures resulting in enhanced turbulent heat fluxes (Fausto et al., 2016), increasing melt can also be attributed to lower surface albedo yielding increased solar absorption (Box et al., 2012), and changes in cloud conditions (Hofer et al., 2017; Orsi et al., 2017; van Tricht et al., 2016). The complexity of ice sheet melt makes the full energy balance approach necessary to diagnose the drivers of that melt.

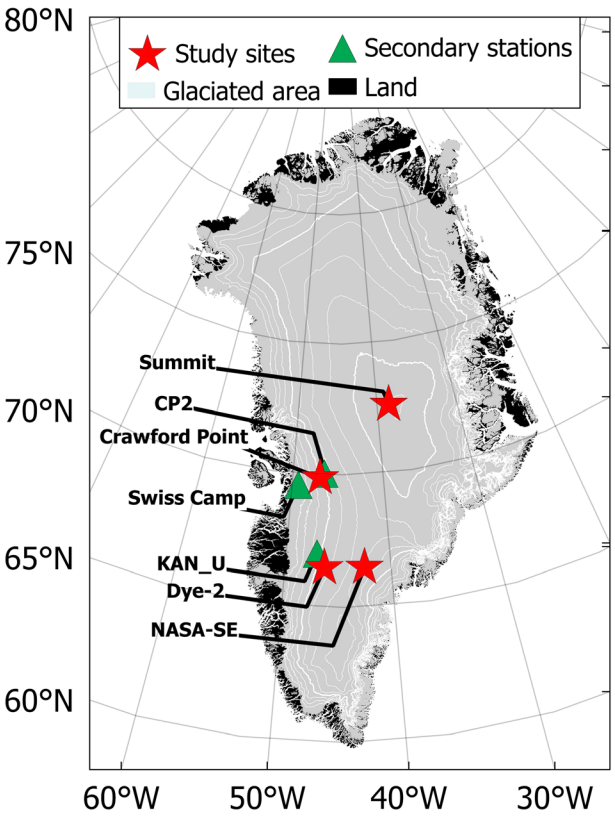

Figure 1. Locations of the study sites and secondary weather stations used for gap-filling. Ice sheet elevation contours are shown every 250 m with thicker lines indicating the 2,000- and 3,000-m elevations above sea level.

The upward migration of melt area presents an additional challenge owing to the limited observational climate records available for calculating the surface energy and mass balances in the accumulation area, over decadal time scales. The firn covering these regions also has the ability to retain surface meltwater (Pfeffer et al., 1991), complicating runoff calculations compared to over bare ice in the ablation area where meltwater is typically assumed to run off. Recent studies have investigated processes influencing firn structure and porosity in the accumulation area of the ice sheet (de la Peña et al., 2015; Forster et al., 2014; Harper et al., 2012; Machguth et al., 2016; van Angelen et al., 2013). Among them, De la Peña et al. (2015) and Machguth et al. (2016) reported an increase in near-surface firn density and ice content as a consequence of increased meltwater production. However, no observed climate histories were available at their sites, making it difficult to investigate the drivers of firn densification thoroughly.

Recent advances in firn modeling facilitated a move from empirical parameterizations of meltwater retention based on few climate parameter (Janssens & Huybrechts, 2000; Reijmer et al., 2012) to physical multilayer snow and firn models resolving multiple subsurface processes driven by weather observations (Charalampidis et al., 2015; Marchenko et al., 2017; Wever et al., 2014; Wever et al., 2016) or regional climate models (Langen et al., 2017; Steger et al., 2017). These models now allow identifying the contributions of various subsurface processes to a net observable change in firn structure and density and therefore allow a better understanding of the surface of the Greenland ice sheet and of its response to climate warming. Yet these firn models have seldom been forced by observed climate and validated against field measurements on the Greenland ice sheet. As a result, though the drivers of changes in the firn have been known for decades, the exact magnitude of their contribution to the near-surface firn density evolution remained unknown.

In this study, we identify and quantify the action of the main drivers of firn density at four sites located in different climate zones of the accumulation area of the Greenland ice sheet, using a multilayer firn model that simulates the processes affecting firn density. The model is forced by the surface mass and energy fluxes calculated from processed and gap-filled automatic weather station data. To ensure the reliability of the firn model, its results are validated against independent observations of density in 22 firn cores. Evolution of the surface climate and energy fluxes are also discussed.

2. Methods

2.1. Climate Station Data and Gap Filling

The observational data that drive the surface energy balance model are gathered by four Greenland Climate Network (GC-Net) stations (Steffen et al., 1996; Steffen & Box, 2001): Crawford Point, Dye-2, NASA-SE, and Summit (Figure 1 and Table 1). We use hourly values for net shortwave radiation fluxes, air temperature, humidity, and wind speed at one of the two levels available on GC-Net stations. We use primarily the higher-level instruments, less prone to be buried under accumulating snow, and use the lower-level instruments only when data from the upper instruments are unavailable. We do not use data recorded at less than 0.5 m from the surface or at unknown height. Due to the harsh climate and 1–2-year revisit times, GC-Net station data can be subject to prolonged multimonth gaps due to instrument or power failures. The data availability after discarding erroneous values is listed in Table 2. We interpolated over gaps under 6 hr, but for larger gaps in temperature, relative humidity, wind speed, and downward shortwave radiation, secondary weather station data were used (Figure 1 and Table 1). Third-level gap filling, when necessary values were unavailable from secondary stations, data from the closest grid cell of the high resolution (0.05° × 0.05°) HIRHAM5 regional climate model (Lucas-Picher et al., 2012) forced by ERA-Interim reanalysis data set (Dee et al., 2011) are used as our best estimation of climate variable at the main station.

Table 1
Overview of Study Site Locations, Periods Considered in This Study, and Secondary Weather Stations Used for the Gap-Filling Procedure

Name	Latitude (°N)	Longitude (°W)	Elevation (m a.s.l.)	Period	Main station (distance)
Crawford Point	69.879	46.986	2022	1998–2010	
Dye-2	66.480	46.279	2165	1998–2015	
NASA-SE	66.481	42.322	2360	1998–2015	
Summit	72.580	38.504	3208	2000–2015	
CP2	69.879	46.986	1990	1997–1999	Crawford Point (6.5 km)
Swiss Camp	69.568	49.316	1149	1994–2015	Crawford Point (97 km)
KAN_U[a]	67.000	47.024	1840	2009–2015	Dye-2 (67 km)

[a]Station from the Greenland analogue project (GAP) and Programme for monitoring of the Greenland ice sheet (PROMICE) network (Ahlstrøm et al., 2008).

Because they come from different locations, heights or sources, each variable in the auxiliary data (secondary station or HIRHAM5) needs adjustment, to match at best the available data from the main station, before they are used for gap-filling. Other studies have used linear functions (Charalampidis et al., 2015; Tardivo & Berti, 2012), but this approach applies the same linear function on all values of the variable to be adjusted and can lead to unrealistic adjusted values (see supporting information). To allow more flexibility, we adjust the auxiliary data using piecewise spline functions so that adjustment is done differently for six intervals spanning from the lowest to the highest value of the auxiliary data. Auxiliary data adjusted using piecewise spline functions give a better match to the available data from the main station than auxiliary data adjusted using linear functions. We therefore believe that our approach will give more realistic values over the periods when they are used to gap-fill the main station records. More information is available in the supporting information.

Gaps in upward shortwave radiation are dealt with differently as surface albedo depends strongly on the local conditions of the snow (grain size, frequency of precipitation, or melt events). Therefore, we use daily surface albedo from the nearest cell in the Moderate Resolution Imaging Spectroradiometer (MODIS) MOD10A1 data after Box et al. (2017) and multiply it by downward shortwave radiation to get the upward radiative flux. Before year 2000, when MOD10A1 data are unavailable, we use the daily averaged climatological albedo value from the MOD10A1 data set for gap filling.

Downward longwave radiation is not measured by the GC-NET stations. It is therefore reconstructed from HIRHAM5 data for the entire period. We found that HIRHAM5 underestimates downward longwave radiation at all 21 stations from the Programme for Monitoring of the Greenland Ice Sheet (PROMICE) (Ahlstrøm et al., 2008). All PROMICE stations are located on the margin of the ice sheet and at low elevation ($<$1300 m a.s.l. except KAN_U at 1,840 m a.s.l.) and in the absence of distributed longwave radiation measurement in the interior of the ice sheet the mean bias at PROMICE sites (-14 ± 5 W/m^2) is used to correct the HIRHAM5 downward longwave radiation at all study sites.

The gap-filled data are presented in Figures S2–S5 in the supporting information, and gap-filling statistics are given in Table S1.

Table 2
Data Availability at the Four Weather Station Sites (%)

	Crawford point	Dye-2	NASA-SE	Summit
Downward shortwave radiation	86	87	84	84
Upward shortwave radiation	78	76	79	81
Air temperature	90	95	82	92
Relative humidity	90	95	79	91
Air pressure	1.5	33	82	86
Wind speed	88	88	74	84
Surface height	96[a]	93	80	96

[a]Including surface height record from CP2.

The weather stations also measure surface height change which can be used to calculate hourly solid precipitation (Charalampidis et al., 2015). This method consists in smoothing the surface height record to remove transient deposition and erosion events and considers every sustained increment in surface height as a new layer of snow. The density of the snow that composes these increments was assumed to be 315 kg/m^3 after Fausto et al. (2018). However, the addition of new snow at the surface immediately triggers compaction within the deposited snow and in the underlying snow and firn, which means that the increment seen by the weather station is only part of what has been deposited. The calculated accumulation record thus underestimates snowfall. This was confirmed by comparing the cumulated snowfall calculated at the station to the end-of-winter snow water equivalent (SWE) surveyed occasionally at the study sites (see Figure S6 in the supporting information). Charalampidis

et al. (2015) compensated this underestimation using higher new snow density (400 kg/m^3) but the data available at each site and in Fausto et al. (2018) indicate that such near-surface snow density is not realistic. We, on the contrary, attribute this underestimation to the compaction of snow and firn below a newly deposited snow layer and apply a correction factor to each increment found in the snow height record. This correction factor is tuned at each site so that the weather station-derived end-of-winter SWE matches the ones reported in snow pits (see Figure S6 in the supporting information). During data gaps (see Table 2) snowfall from HIRHAM5 output, multiplied by a correction factor to match the available station-derived accumulation, is used instead.

2.2. Surface Energy Balance Model

Surface energy and mass fluxes are calculated using the model by van As et al. (2005) which has been previously used on weather station data on the Greenland ice sheet (Charalampidis et al., 2015; van As et al., 2017). At each hourly time step, it calculates the turbulent latent and sensible heat fluxes from near-surface gradients in air temperature, humidity, and wind speed using Monin-Obukhov similarity theory accounting for thermal stratification effects on the logarithmic wind speed profile. Surface roughness length scales are parameterized as a function of surface snow density (Andreas, 1987; Lefebre et al., 2003). The model iteratively searches for a surface temperature below or equal to 0 °C for which all surface energy fluxes are in balance. Upwelling longwave radiation is calculated from simulated surface temperature using Stefan-Boltzmann's law with an emissivity of 0.98. Conductive heat flux into the subsurface is calculated from the temperature gradient across the first layer in the firn model (see next section). Since the surface is composed of snow or ice, the surface temperature is limited to 0 °C, and any excess energy required to close the energy budget is used to melt of snow or ice. Sublimation and deposition are calculated from the latent heat flux.

2.3. Firn Evolution Model

The snow and firn model employed here was first presented by Langen et al. (2015), and was updated in Langen et al. (2017). In this section, we give a brief summary of the model from Langen et al. (2017) and describe further improvements made to the model since then.

2.3.1. Discretization

The firn column is here composed of 200 layers, each of which consists of three compartments: snow, pure ice, and liquid water. Layer temperature, firn grain size, and firn density are calculated for each layer. Langen et al. (2017) implemented an Eulerian approach, whereby added or removed mass was going through fixed layers of constant mass. This resulted in systematic averaging of the firn properties. In this study, we have updated the discretization scheme to allow layers to be advected downward or upward in a Lagrangian fashion. New layers containing snow can be created at the surface during precipitation events. New ice layers can be added at the bottom of the column if the thickness of the entire column drops below 20 m water equivalent (w.eq.). Surface layers can also disappear as the surface melts, while the deepest layer can be removed once buried too deep. To maintain a constant number of layers, the creation (respectively, deletion) of a layer is balanced by merging (respectively, splitting) of layers elsewhere in the column. Merging or splitting layers are done so that vertical resolution is higher close to the surface and that layers having significantly different characteristics (in temperature, density, ice and water content, grain size) than neighboring layers are less likely to be merged with others.

2.3.2. Mass Fluxes

An update since Langen et al. (2017) is that new material from snowfall or deposition is now first kept in a fresh snow bucket, and only when this bucket reaches a specified threshold (4 cm w.eq.), a new layer is created. The fresh snow bucket is used to distinguish fresh snow from old snow, information needed for the parameterization of surface roughness length from Lefebre et al. (2003). A fresh snow density of 315 kg/m^3 after Fausto et al. (2018), which already accounts for the effect of wind, is preferred to the parameterization used in Langen et al. (2017). Grain size of fresh snow is set to 0.1 mm as in Langen et al. (2017) and Katsushima et al. (2009). When sublimating or melting material, it is first taken from the fresh snow bucket and then from the first layer of the column. Melting at the surface triggers the transfer of the content of the fresh snow bucket to the first layer and thereafter shifts mass from the snow and ice compartments to the liquid water compartment.

2.3.3. Meltwater Percolation and Refreezing

The way water is passed from one layer to the next is unchanged from Langen et al. (2017). After calculating what can be retained by capillary forces, the excess water is available for downward movement following Darcy's law and depending on the conditions (density, grain size, and ice content) that are present in the two considered layers. Once the water movement is calculated for the whole column, the cold content of the subfreezing layers is used to refreeze the liquid water (including as superimposed ice). Firn compaction and grain growth are also unchanged since Langen et al. (2017).

As a minor update, we chose to use the formulation of saturated hydraulic conductivity after Calonne et al. (2012) and use the parameterization of heat capacity and thermal conductivity from firn density after Yen (1981). Finally, the parameterization from Colbeck (1975) is used to describe how discontinuous ice lenses decrease the snow hydraulic conductivity. The scheme requires a standard ratio between the width of gaps separating ice lenses and the width of ice lenses, $\frac{w_h}{w_{ice}}$, and although Langen et al. (2017) used both 1 and 0.1, they did not provide any justification. Here we argue that $\frac{w_h}{w_{ice}} = 0.1$ is more meaningful as it allows a layer filled by ice to have a hydraulic conductivity one order of magnitude lower than ice-free snow and therefore to be closer to observations of ice layer conductivity in natural snowpacks (Albert & Perron, 2000).

2.3.4. Model Initialization

The model starts with an initial column of 40 m w.eq. We use the closest available firn cores in time and space to initiate the firn density. At Dye-2 and NASA-SE, we use core Dye-2 A&B and core 6642 (120 and 20.13 m long, respectively) from Mosley-Thompson et al. (2001). At Crawford Point, no core drilled at that site in the 1990s was available. We therefore use the 18.55-m-long core 6945 drilled in 1998, 125 km southeast of the site, and 189 m higher on the ice sheet (Mosley-Thompson et al., 2001). The two locations are assumed to have the same firn condition. It is corroborated by other studies that already compared core 6945 to snow pits from the surroundings of Crawford Point (de la Peña et al., 2015). At Summit the initial density was taken from a 6-m-deep snow pit by Mayewski and Whitlow (2016) and the GRIP core (Spencer et al., 2001), both from 1990, when usable station data only start in 2000. Nevertheless, an ~2-m snow pit from 2000 by Albert and Shultz (2002) (see Figure S8 in the supporting information) indicates that shallow firn densities were similar in 1990 and 2000 and justifies our choice of initial condition. For Crawford Point and NASA-SE the density from the end of the available core to the bottom of the column is calculated by fitting a second-degree polynomial to the available density and to a pore close off density (830 kg/m^3) at 30 m w. eq. (~60 m) below the surface and then constant from there.

The initial temperature profile was taken as the first valid reading of the temperature strings that are installed at the GC-Net stations. Since the lowest-temperature sensor is located at ~10-m depth, the rest of the temperature profile is calculated using a second-degree polynomial to link the lowest available temperature to the bottom temperature. This bottom temperature is kept constant throughout the simulation and is set to the average firn temperature at 10-m depth observed by the thermistor string installed at each station: −17.4 °C at Crawford Point, −16.0 °C at Dye-2, −19.2 °C at NASA-SE, and −31.0 °C at Summit station.

3. Results

3.1. Climate Forcing, Energy, Mass, and Water Budget

We have compiled 12 to 17 years of climate data per study site, which give unprecedented insight into the evolution of the climate in the accumulation area of the Greenland ice sheet. Clear trends were seldom found throughout all variables monitored by the stations. For all study periods, the GC-Net stations show slight increase in annual and summer mean air temperature, congruent with climate change induced trends found, among others, by Hanna et al. (2008). However, probably due to the length of the considered records with respect to the natural variability, these trends cannot be proven statistically different from zero (all of them have p value >0.1; see Table S2 in the supporting information). The warming was noticeably more pronounced (higher slopes, smaller p values) for summer averages than for annual means.

As a key parameter of the surface energy balance, the evolution of the surface albedo was also investigated. The June through August average albedo was consistent between the sites (~0.83) and stable at Dye-2, NASA-SE, and Summit (Figure S7 in the supporting information). Yet albedo during the summer of 2012

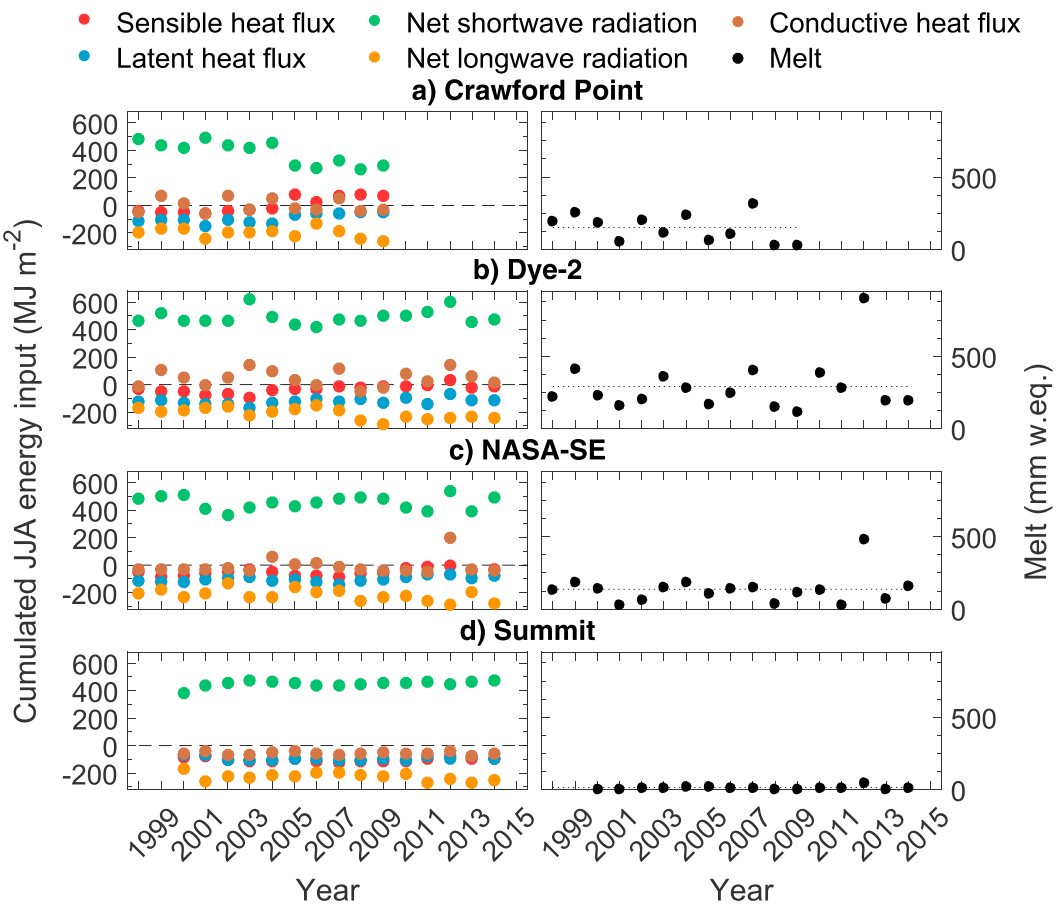

Figure 2. (left panels) Surface energy input summed June through August (JJA) each year. (right panels) Cumulated yearly surface melt. Dashed line on the left indicates zero energy input to the surface and segregate energy sinks (negative input) from energy sources (positive input). Dotted line on the right shows the average annual melt amount at each site. The similar magnitudes of latent and sensible heat fluxes at summit (d) cause the overlap of their markers.

was record-low at Dye-2 (0.75 ± 0.05) and NASA-SE (with 0.78 ± 0.05). At Crawford Point, summer albedo was on average 0.05 higher during 2005–2009 compared to 1998–2004 translating into a decreasing energy input of net shortwave radiation to the surface (Figure 2 and Table 3). This increase was not found in MODIS summer albedo; however, no malfunction was reported for that period in the station data. It is therefore difficult to ascertain the origin of this increase.

The calculated surface energy balance, illustrated in Figure 2, reveals the diversity of processes that govern the surface energy and mass budgets. For all sites, net shortwave radiation is the largest heat source and net longwave radiation is the largest heat sink for the surface during summer (Figure 2). In 2012, both at Dye-2 and

Table 3
Trends in the Components of the Surface Energy Balance

	Sensible Heat Flux	Latent Heat Flux	Net Shortwave Radiation	Net Longwave Radiation	Conductive Heat Flux
	Trends in cumulated JJA energy (MJ/m^2/year)				
Crawford Point	**14.09**	**7.25**	**−20.09**	−3.4	−2.16
Dye-2	**4.02**	**2.09**	1.25	**−5.28**	0.16
NASA-SE	**2.75**	**2.53**	−0.36	**−4.32**	2.38
Summit	0.02	−0.36	2.69	−3.10	−0.37

Note. Trends significantly different from zero (i.e., with associated p value <0.05) are shown in bold. Positive values indicate energy fluxes that heat the surface.

NASA-SE, surface melting led to lower albedo values (Figure S7 in the supporting information), causing increased shortwave radiation absorption (Figure 2) through the melt-albedo feedback (Box et al., 2012).

Our calculations of sensible and latent heat fluxes are in agreement with previous estimates using similar methods (Box & Steffen, 2001), and their cumulated June through August values are increasing at all sites except Summit (Table 3). However, Box and Steffen (2001) also described a possible negative bias when calculating sublimation from a single height above the surface. Using more advanced methods, such as the so-called eddy covariance method would be indeed preferable, but is hampered by the scarceness of periods where temperature, humidity, and wind speeds are available at two levels above the surface.

Longwave radiation fluxes are decreasing at all sites. But since downward longwave radiation is provided by HIRHAM5, this result is not based on direct observations from the weather stations. Conductive heat fluxes through the uppermost snow layer show a more mixed picture, and it seems that the capacity of the near-surface firn to accept heat from the surface did not drastically change at any site over the study period. Investigation of the heat conducted through the model column showed that only the near-surface firn was thermally active. Subsequently, the assigned bottom temperature, which could in theory act as an infinite source or sink of heat, did not interfere with the near-surface heat fluxes and latent heat release from refreezing.

Higher surface melt was calculated over the last decade (Figure 2), especially during the known extreme melt events of 2007 (Mote, 2007), 2010 (van As et al., 2012), and 2012 (Nghiem et al., 2012). The relatively short span of our records prevents from calculating trends representative of current climate evolution. However, a recent ice core study by Graeter et al. (2018) found that melt indeed increased at Crawford Point and Dye-2 over the last 50 years. But while Graeter et al. (2018) estimated surface melt from ice content in firn cores, subject to high spatial variability, our calculation of surface melt from the weather station data presents a more robust estimate.

Mean annual snowfall was respectively 564, 421, 731, and 303 mm w.eq. at Crawford Point, Dye-2, NASA-SE, and Summit over their respective study periods. At all sites, the meltwater is entirely refrozen in the snow and firn. The only modeled process removing mass from the firn column is sublimation, which on average sublimated 6.7%, 12.8%, 6.8%, and 12.2% of annual snowfall at Crawford Point, Dye-2, NASA-SE, and Summit, respectively. We calculate an average annual mass balance of 526, 367, 681, and 266 mm w.eq. at Crawford Point, Dye-2, NASA-SE, and Summit, respectively.

3.2. Firn Evolution and Densification

At sites where surface melt is frequent such as Crawford Point, Dye-2, and NASA-SE, ice layers are being formed from meltwater refreezing every summer. This is visible in Figure 3 as layers of higher density. Snow densifies with time as it gets buried under new material, with fastest compaction rates in the few months following snowfall. Additionally, Crawford Point and Dye-2 start with very few high-density layers in the upper 10 m while they end their respective study periods with a higher number of them in the near-surface firn. Seemingly abrupt changes in density at depth in Figure 3 are the result of the model layers merging in order to add new ones at the top.

4. Discussion

4.1. Evaluation Against Firn Cores

Before we further discuss the simulated evolution of the firn we need to assess the accuracy of the model. Errors on the initial conditions, from the climate forcing and limitations of the model formulation, affect the ability of the model to simulate the firn evolution. We assess the net effect of all these inaccuracies by comparing the modeled densities to 22 firn density observations. Among them 14 were already published (Albert & Shultz, 2002; Harper et al., 2012; Lomonaco et al., 2011; Machguth et al., 2016) while 8 are being presented for the first time (core 3 to 6 at NASA-SE and 22 to 25 at Summit; see Figure S8 in the supporting information) and have a 10-cm resolution in density.

For each core we calculate the average density for the whole core, for its upper section (above 5-m depth) and for its lower section (below 5-m depth) and compare it to the average densities given by the model at the same date and same depth range. When compared to the full cores, the simulations give a satisfactory

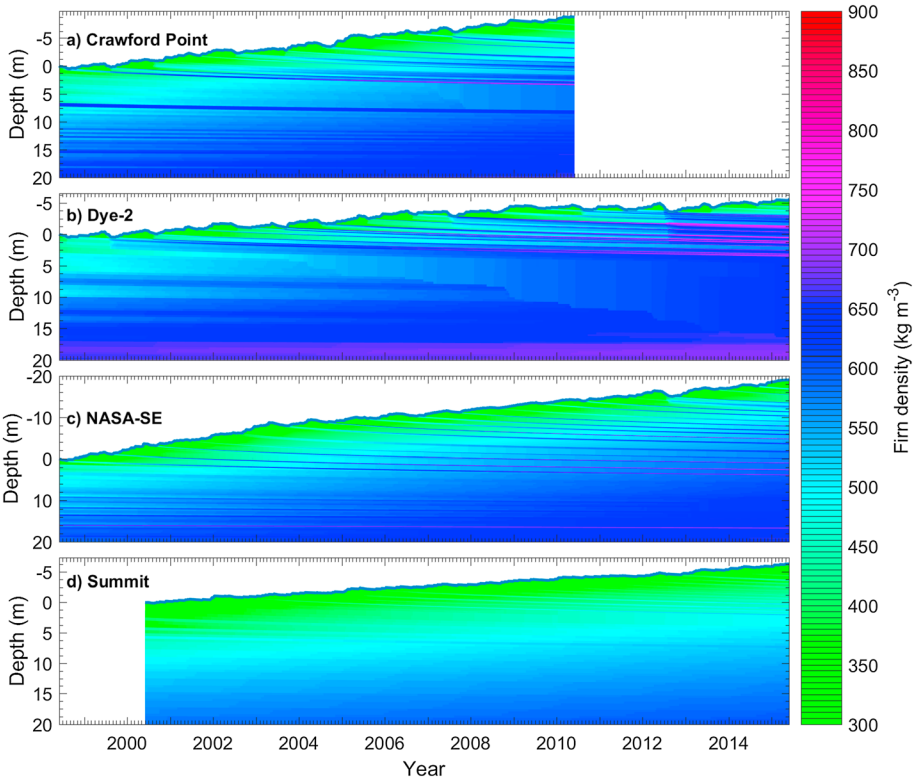

Figure 3. Evolution of simulated firn density at four GC-Net sites. Steps in density evolution between 5 and 10 m deep at Crawford point and Dye-2 are due to the model merging layers and to the averaging of their density. It is done so that new layers are available closer to the surface.

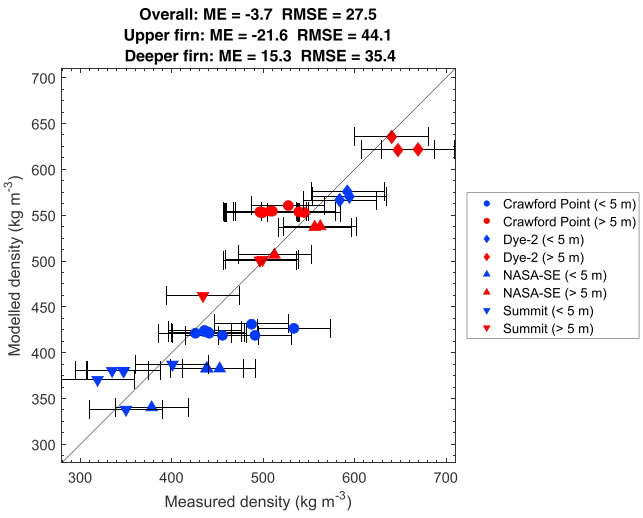

Figure 4. Evaluation of modeled and observed average firn density for the four sites for shallow (<5 m; in blue) and deep (>5 m; in red) firn. Mean error (ME) and root-mean-square error (RMSE) on the average densities are given for the whole depth range covered by the cores (overall), for the core sections within 5 m from the surface (upper firn), and for the core sections below 5-m depth (deeper firn).

mean error (ME) of −3.7 kg/m^3 and root-mean-square error of 27.5 kg/m^3 (Figure 4). However, the model on average underestimates the upper-firn average density by −21.6 kg/m^3 and overestimates the deeper-firn average density by 15.3 kg/m^3 (Figure 4). These discrepancies are most likely due to the densification scheme (Vionnet et al., 2012) that was designed for seasonal snowpack and not for polar firn, but also to inaccurate melt or snowfall at the surface or limitations in the meltwater percolation scheme in the firn model. Nevertheless, deviations between modeled and observed average firn densities are well within the natural variation of firn density at local scale due to spatial heterogeneities (standard deviation of the average densities from nine cores drilled in 2007 at Crawford Point is 23.1 kg/m^3).

The comparison of the modeled and observed full-depth density profiles (Figure S8 in the supporting information) confirms the agreement of average density and also shows that the model can reproduce denser melt layers within the firn. The model fails, however, to reproduce the exact depth and thickness of these layers. In addition to the sources of discrepancies listed above, the mismatch between modeled and observed ice layers can be due to the inability of the model to account for heterogeneous percolation (Marsh & Woo, 1984). Nonetheless, the objective of this study is to simulate the evolution of the average density of the near-surface firn and to quantify the contributions of surface processes to these changes. We consider that inaccuracies in the modeled depth of the ice layers are not relevant. Indeed, our simulations match reasonably well with observed firn density profiles and represent a likely evolution of the firn in

Table 4
Evolution of Firn Density at the Study Sites From Observations in Firn Cores and From the Model

Site	Period	Depth Range	Density Change (kg/m^3)	
			Observed	Modeled
Crawford Point	1998–2007[a]	0–10.4 m	+24	+16
	1998–2010	0–20 m	–	+ 10
Dye-2	1998–2013[a]	0–16.6 m	+109	+78
	2013[a]–2015[a]	0–16.6 m	−23	0
	1998–2015	0–20 m	–	+ 59
NASA-SE	1998–2015	0–16.6 m	+13	−21
	1998–2015	0–20 m	–	−19
Summit	2000[b]–2007	0–20 m	+8	+5
	2007–2015[a]	0–15.9 m	−19	−1
	2000–2015	0–20 m	–	+1

[a]Average of multiple cores. [b]In fact using the 1990 cores from Spencer et al. (2001) and Mayewski and Whitlow (2016) that appear to match with a 2-m pit from 2000 (Figure S8 in the supporting information).

the vicinity of the weather station. Substantial improvement in climate observation, energy balance modeling, and firn modeling as well as in our understanding of spatial heterogeneity will be needed before we can aim at replicating a mirror image of one specific measurement of density profile.

Beyond the comparison of density profiles at specific dates, it is also important to assess whether the model is able to reproduce the changes observed in firn between two measurements of firn density. Firn cores indicate that the highest densification took place at Dye-2 over the 1998–2013 period (Table 4). However, all the other density changes derived from firn core comparison are rather low compared to the natural spatial variability in firn density. Nevertheless, we believe that, despite spatial heterogeneity, if similar changes in density can be seen between two firn cores and in our simulation (which is the product of our current understanding of the firn processes applied to observed climate data), then there is a higher chance that both reflect the true evolution of the firn. When changes in density given by firn cores and by our simulations differ either in sign or magnitude then we cannot distinguish between potential anomaly in the observations and errors in the forcing or formulation of the firn model. Our firn model captures the sign and magnitude of observed changes: highest increase in density at Dye-2, mild increase at Crawford Point, and little changes at Summit (Table 4). Only at NASA-SE, the model indicates an overall decrease in density while the firn cores showed a small increase of firn density over the 1998–2015 period (Table 4).

4.2. Evolution of the Firn

After ensuring that the firn model gives a realistic estimate for the evolution of firn density, we can now focus on the temporal evolution of the average density of the upper 20 m of firn. This is a key parameter for the firn retention capacity. Simulations show the highest densification at the Dye-2 with an increase of +59 kg/m^3 (+11%) in the density of the upper 20 m of firn from 1 June 1998 to 1 June 2015, respectively (Table 4). The repeatedly positive annual changes of firn density in the second half of the study period (black line above 0 in Figure 5b) indicate that this increase in density started in 2006. Increasing density at Dye-2 causes the loss of 18% of the firn pore volume and represents a substantial decrease of the meltwater storage capacity of the firn. Crawford Point and Summit show rather stable densities (changes lower than 2%). However, no data are available at Crawford Point after 2010 and considering the similarities of their location (in western Greenland, ~2,000 m a.s.l.), it cannot be excluded that the site underwent the same densification, and loss of pore volume, as Dye-2 over the 2010–2015 period.

More surprisingly, our simulation at NASA-SE shows a 19 kg/m^3 (4%) decrease of firn density. The decrease in near-surface firn density primary occurs between 1998 and 2003 and is followed by a period of stable firn densities (Figure S9 in the supporting information). Calculated year-to-year changes in firn density (Figure 5, black line) indicate that this decrease can be attributed to higher precipitation than average. No major issue potentially affecting the station-derived precipitation was reported over that period, and unfortunately, no firn core was drilled at NASA-SE between 1998 and 2015 to assess whether this decrease of firn density indeed took place.

Although the firn core observations used for the initialization of the firn density cover the upper 20 m at all sites, our analysis naturally depends on the uncertainty present in these initial profiles. Nevertheless, the effect of any measurement error within these profiles would decrease throughout the simulation as the anomalous firn section is advected out of the upper 20 m of firn. Measurement errors put aside, the natural spatial heterogeneity of firn raises the question of representativity of the initial profiles that were used. In the absence of clear understanding of spatial heterogeneity and of its potential controls, we can only aim at simulating the likely evolution of the firn at the specific location where the initial density profiles were observed.

4.3. Drivers of Firn Density

It is known that near-surface firn density tends to decrease in periods of high precipitation and/or low melt (e.g., at NASA-SE during 1998–2003; Figure S9 in the supporting information) and to increase in periods of

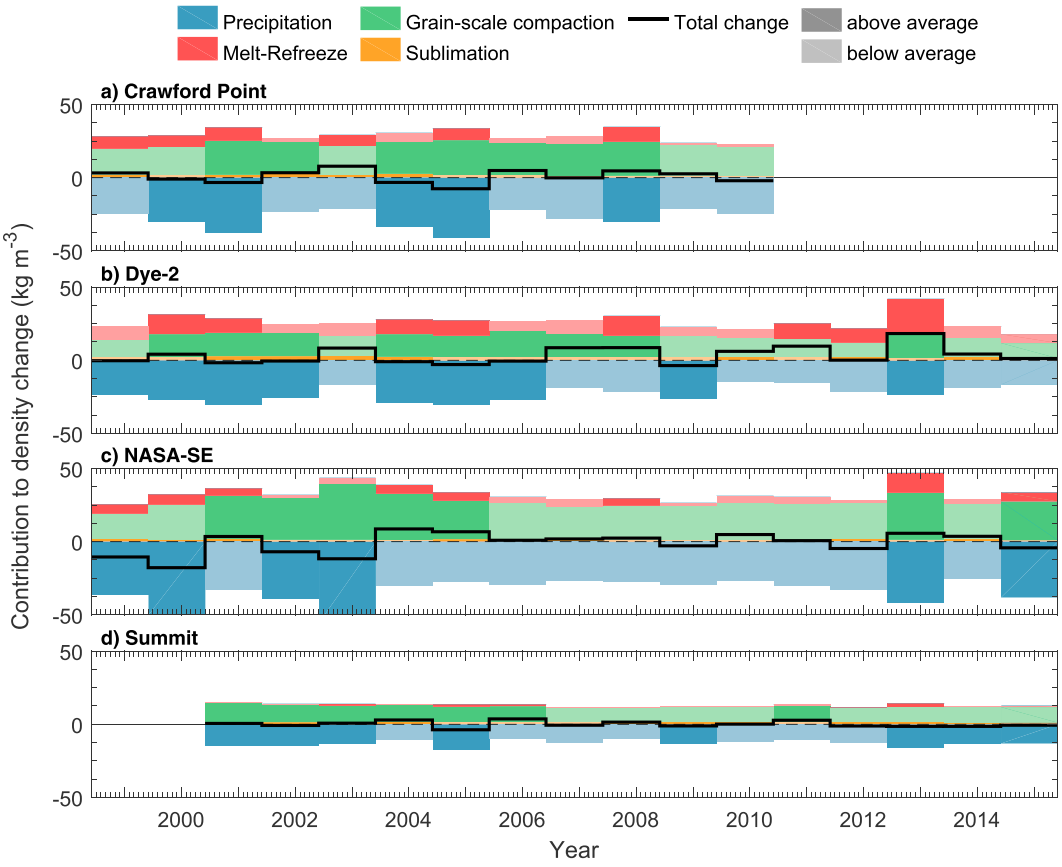

Figure 5. Temporal evolution of the near-surface firn (upper 20 m) density and of its drivers at (a) Crawford point, (b) Dye-2, (c) NASA-SE, and (d) Summit. Annual change in 20-m firn density (from 1 June to 1 June) is shown in black line, and the contribution of densification processes are shown in stacked colored areas (with darker colors when contributions are above whole-period average).

lower precipitation and/or higher melt (e.g., at Dye-2 over the 2007–2015; Figure S9 in the supporting information). Snowfall adds less dense fresh snow at the top of the firn column subsequently decreasing the average density of the upper 20 m of firn. On the contrary, surface melt transforms less dense surface snow into ice layers at depth thereby increasing the firn density. Two other processes affect near-surface firn density: the grain-scale compaction, which sinters and recrystallizes snow grains in response to the overburden pressure (and thereby to precipitation and melt history), subsurface temperature and water content (calculated after Vionnet et al., 2012) and sublimation at the surface, which by removing less dense surface snow will increase the average density of the upper 20 m of firn that remains. The firn model brings new insights by giving the magnitude of the near-surface density change related to precipitation, melt, compaction, or sublimation at each time step.

First, the hourly contributions can be aggregated into yearly contributions (i.e., from 1 June to 1 June) so that we can identify, for each year, the main driver of changes in the near-surface firn density (Figure 5). In addition to the magnitude of the contributions, we also show in Figure 5 whether that contribution is below (lighter color) or above (deeper color) the average contribution for the whole period. From Figure 5, we can therefore investigate and quantify, for each year, each driver's contribution the interannual change in near-surface firn density.

The role of precipitation for all sites is evident as shown in Figure 5. Year-to-year decrease in firn density (black line below zero in Figure 5) only comes with above-average precipitation (deep blue colored areas in Figure 5). On the contrary, below-average precipitation always leads to increasing firn densities. These two statements have one exception: at NASA-SE over 2010–2011, but are otherwise supported by 53 combined -station-years.

Table 5
Part of the Variance in Near-Surface Density Change Explained by the Contribution of Each Driver of the Top 20-m Firn Density, Calculated Both on Daily and Yearly Values (From 1 June to 1 June)

		Part (%) of the Variance in Near-Surface Density Change Explained by the Individual Contribution of			
Site	Temporal Scale	Precipitation	Melt	Grain-Scale Compaction	Sublimation
Crawford Point	Daily	84	19	9	7
	Yearly	68	1	14	1
Dye-2	Daily	72	33	17	6
	Yearly	29	43	3	11
NASA-SE	Daily	92	11	5	5
	Yearly	55	3	1	0
Summit	Daily	92	7	3	7
	Yearly	74	6	6	0

Note. Values for each site do not add up to 100 because of covariance between drivers.

While precipitation decreases near-surface firn density, on average by −13 to −34 kg/m^3 each year, it is partly compensated by the grain-scale compaction that densifies the near-surface firn on average by 11 to 26 kg/m^3. The formula by Vionnet et al. (2012) implies that grain-scale compaction decreases exponentially with increasing densities. Therefore, years with more precipitation bring more low-density snow to a site and leads greater grain-scale compaction (Figure 5). The grain-scale compaction is therefore the second contributor to firn density changes in magnitude. Nevertheless, and as detailed in the next section, the response of grain-scale compaction to precipitation is dampened. The variance of the contribution of grain-scale compaction is indeed between 4 and 11 times smaller than the one of snowfall. Therefore, we see that grain-scale compaction moderately counterbalances the contribution of precipitation and does not drive changes in the near-surface firn density over our study periods.

Due to the different locations of the stations, melting and subsequently melt-driven densification does not occur every year at all sites. At Crawford Point and Dye-2, melt and refreezing are responsible for an important part of the increase of near-surface firn density from one year to the next: 20 and 37% of all positive contributions to firn density change on average, respectively. At these sites the variability in melt also has its importance since above average melt years (Figure 5) generally (for 80% of such station-years) cause a positive change on the near-surface density change. At Summit, melt occurs rarely and does not have a significant effect on near-surface firn density. At NASA-SE, however, the contribution of melt and refreezing to the overall densification only becomes important during extreme melt events such as in 2012, when it accounted for a +14 kg/m^3 increase of density which was in turn compensated by an above-average contribution from snowfall.

The role of sublimation is minor for all sites and all years with an average annual contribution of +1.4 to +2.2 kg/m^3 depending on the site.

4.4. Effect of the Temporal Scale on the Drivers of Densification

Another approach to describe the role of precipitation, melt, grain-scale compaction, and sublimation into the evolution of the near-surface firn density is to see how much of the variability, or variance, in the density change can be explained by each driver (Table 5). This is done by calculating the coefficient of determination (R^2) of the linear regression between each driver's contribution and the overall density change.

Figure 5 indicates that precipitation is responsible for the largest and most variable contribution to the interannual evolution of the near-surface firn density. Precipitation also appears to be the main driver of the day-to-day variance in the firn density (Table 5). Due to the difference in average summer melt between the sites, the explanatory power of precipitation decreases, and the one of melt increases, as we move from colder sites (Summit, NASA-SE) to warmer sites (Crawford Point, Dye-2).

The higher values of explained variance at daily resolution, for all drivers of density, comes from the fact that on a day-to-day basis, the changes in density can be more easily linked to one single driver (for example, day of snowfall in absence of melt or melt day without snowfall). On yearly values, however, the drivers explain less of the variability in density (Table 5). This comes from the fact that over annual time scales, drivers contribute simultaneously to interannual changes in the firn density and cannot be separated into their individual contribution. Only at Dye-2 the yearly contribution of melt is still very important and explains 43% of the variance in annual changes in firn density. Yet precipitation alone still explains more than half of the variance in interannual changes of density at all the other sites.

Another argument for the dominant role of precipitation in near-surface density change, is that extreme precipitation events lead to much more drastic changes in the near-surface firn density (from −2 to −6 kg/m^3 within a day due to extreme snowfall) than the extreme melt events (+1.3 kg/m^3 during the strongest melt day at Dye-2). Therefore, when aiming at simulating the daily evolution of firn density, capturing these precipitation events appears to be more important than capturing the variability in any other drivers of densification.

Our conclusions are strengthened by the fact that precipitation and, in a less direct way, melt are calculated from the weather station data and therefore represent our closest estimates of true surface conditions. Additionally, the calculation of their contributions to near-surface firn density change is rather straightforward (adding new snow at the top for precipitation and transforming surface snow to ice for melt) and depends on a limited number of observation-derived assumptions: fresh snow density is taken from Fausto et al. (2018) and no runoff was reported at any of our study sites over the considered periods.

Another interesting finding is the relatively minor importance of the contributions of grain-scale compaction and sublimation into daily and yearly changes in the near-surface firn density (Table 5). It indicates that at our sites, over periods of ~15 years, grain-scale compaction and sublimation (as they are formulated in the firn model) do not vary sufficiently to have a noticeable impact on the evolution of the density of the upper 20 m of firn. Table 5 indicates that the contributions of grain-scale compaction and densification could be replaced by their mean values without losing much explanatory power. This finding is more dependent on the formulation of grain-scale compaction in the model, and on its sensitivity to changes in accumulation, temperature, or water content. It should therefore be used with caution.

All our results indicate the importance of precipitation, and its variability at different temporal scales to estimate the evolution of the near-surface firn density. This highlights the difficulty with attributing observed density changes to changes in melt alone (de la Peña et al., 2015; Graeter et al., 2018).

5. Conclusions

Climate data covering 12–17 years at Crawford Point, Dye-2, NASA-SE, and Summit automatic weather stations and adjusted data from nearby weather stations and HIRHAM5 regional climate model output were combined in continuous hourly time series. A surface energy and mass balance model driven by these data enabled the estimation of the relative contributions of the different surface energy and mass fluxes to the surface. We find that sensible and latent heat fluxes have increased at most sites but were partly compensated by a decrease in radiative fluxes. Melt was seen to be highest at the end of our study period with the occurrence of the 2007, 2010, and 2012 extreme melt events. Our updated snow and firn model revealed that the density of the top 20 m of firn has increased by 11% at Dye-2, subsequently decreasing the firn pore space by 18%. No near-surface firn density increase was found at Crawford Point and Summit while a 4% decrease was found at NASA-SE. Modeled densification is corroborated by comparison with firn cores. We find that precipitation changes are primarily responsible for the modeled variations of firn density at our study sites. Indeed, its contribution to changes in near-surface firn density change is both the highest in magnitude and the most variable of all drivers of firn densification. Precipitation can therefore explain alone 72 to 92% of the variance in day-to-day firn density change while melt can only explain 7 to 33% alone. When looking at year-to-year changes in firn density, precipitation is still the main driver followed by melt, however it is then their interaction that is necessary to explain the evolution of firn density. Contributions of grain-scale compaction and sublimation to the changes in firn density are less important and could not explain much of the variance in firn density change. We nevertheless expect this last finding to be more dependent on the model formulation of grain-scale compaction. Our results are of prime importance for the climate modeling community and provide a strong impetus to reproduce the observed magnitude and variability of precipitation in order to better estimate the past and future evolution of the firn on the Greenland ice sheet. It is also yet another reminder that observed changes in the firn density cannot be attributed entirely to changes in melt or temperatures without an accurate estimation of the precipitation history at that location. Eventually, should the decrease of pore space and buildup of ice layers at Dye-2 continue, its meltwater retention capacity could be eliminated as it has been reported at lower areas in the same region (Machguth et al., 2016), and meltwater generated there could participate to runoff. This possibility reaffirms the necessity of field campaigns and modeling efforts to understand ongoing changes in the firn of the Greenland ice sheet.

Acknowledgments

This work is part of the Retain project funded by the Danmarks Frie Forskningsfond (grant 4002-00234). We are grateful to J. Harper and E. Mosley-Thompson for providing some of the cores used in this study and to A. Heilig, J. Brown, and two anonymous reviewers for their useful comments on the manuscript. The GC-Net data are available at http://cires1.colorado.edu/steffen/gcnet. The data produced by this study (processed gap-filled hourly standardized weather data and SEB and firn model output) are available at http://doi.org/10.18739/A2TH8BM6X. The scripts used for this study are available at https://github.com/BaptisteVandecrux/SEB_Firn_model.git. The PARCA cores are available at http://research.bpcrc.osu.edu/Icecore/data/, and their collection was supported by NASA grants NAG5-5032, 6817, 5031, 6779, NAGW-4248, and NSF/OPP grant 9423530. KAN_U weather station data are funded by the Greenland Analogue Project (GAP), and made available through the Programme for Monitoring of the Greenland Ice Sheet (PROMICE). PROMICE data are freely accessible at http://promice.org. HIRHAM5 output is available at http://prudence.dmi.dk/data/temp/RUM/HIRHAM/.

References

Ahlstrøm, A., Gravesen, P., Andersen, S., van As, D., Citterio, M., Fausto, R., et al. (2008). A new programme for monitoring the mass loss of the Greenland ice sheet. *Geological Survey of Denmark and Greenland Bulletin*, *15*, 61–64.

Albert, M., & Shultz, E. (2002). Snow and firn properties and air–snow transport processes at summit, Greenland. *Atmospheric Environment*, *36*(15-16), 2789–2797. https://doi.org/10.1016/S1352-2310(02)00119-X

Albert, M. R., & Perron, F. (2000). Ice layer and surface crust permeability in seasonal snow pack. *Hydrological Processes*, *14*(18), 3207–3214. https://doi.org/10.1002/1099-1085(20001230)14:18<3207::AID-HYP196>3.0.CO;2-C

Andreas, E. L. (1987). A theory for the scalar roughness and the scalar transfer coefficients over snow and sea ice. *Boundary LayerMeteorol*, *38*(1-2), 159–184. https://doi.org/10.1007/BF00121562

Box, J. (2013). Greenland ice sheet mass balance reconstruction. Part II: Surface mass balance (1840–2010). *Journal of Climate*, *26*(18), 6974–6989. https://doi.org/10.1175/JCLI-D-12-00518.1

Box, J., & Steffen, K. (2001). Sublimation on the Greenland ice sheet from automated weather station observations. *Journal of Geophysical Research*, *106*(D24), 33,965–33,981. https://doi.org/10.1029/2001JD900219

Box, J. E., Fettweis, X., Stroeve, J. C., Tedesco, M., Hall, D. K., & Steffen, K. (2012). Greenland ice sheet albedo feedback: Thermodynamics and atmospheric drivers. *The Cryosphere*, *6*(4), 821–839. https://doi.org/10.5194/tc-6-821-2012

Box, J. E., van As, D., Steffen, K., & the PROMICE team (2017). Greenland, Canadian and Icelandic land-ice albedo grids (2000–2016). *Geological Survey of Denmark and Greenland Bulletin*, *38*, 53–56.

Calonne, N., Geindreau, C., Flin, F., Morin, S., Lesaffre, B., Roscoat, S. R., & Charrier, P. (2012). 3-D image-based numerical computations of snow permeability: Links to specific surface area, density, and microstructural anisotropy. *The Cryosphere*, *6*(5), 939–951. https://doi.org/10.5194/tc-6-939-2012

Charalampidis, C., van As, D., Box, J. E., van den Broeke, M. R., Colgan, L. T., Doyle, S. H., et al. (2015). Changing surface-atmosphere energy exchange and refreezing capacity of the lower accumulation area, West Greenland. *The Cryosphere*, *9*(6), 2163–2181. https://doi.org/10.5194/tc-9-2163-2015

Colbeck, S. (1975). A theory of water flow through a layered snowpack. *Water Resources Research*, *11*(2), 261–266. https://doi.org/10.1029/WR011i002p00261

de la Peña, S., Howat, I. M., Nienow, P. W., van den Broeke, M. R., Mosley-Thompson, E., Price, S. F., et al. (2015). Changes in the firn structure of the western Greenland ice sheet caused by recent warming. *The Cryosphere*, *9*(3), 1203–1211. https://doi.org/10.5194/tc-9-1203-2015

Dee, D. P., Uppala, S. M., Simmons, A. J., Berrisford, P., Poli, P., Kobayashi, S., et al. (2011). The ERA-interim reanalysis: Configuration and performance of the data assimilation system. *Quarterly Journal of the Royal Meteorological Society*, *137*(656), 553–597. https://doi.org/10.1002/qj.828

Enderlin, E., Howat, I. M., Jeong, S., Noh, M.-J., van Angelen, J., & van den Broeke, M. (2014). An improved mass budget for the Greenland ice sheet. *Geophysical Research Letters*, *41*, 866–872. https://doi.org/10.1002/2013GL059010

Fausto, R. S., Box, J. E., Vandecrux, B., van As, D., Steffen, K., MacFerrin, M., et al. (2018). A snow density dataset for improving surface boundary conditions in Greenland ice sheet firn modelling. *Frontiers in Earth Science*, *6*(51). https://doi.org/10.3389/feart.2018.00051

Fausto, R. S., van As, D., Box, J. E., Colgan, W., Langen, P. L., & Mottram, R. H. (2016). The implication of nonradiative energy fluxes dominating Greenland ice sheet exceptional ablation area surface melt in 2012. *Geophysical Research Letters*, *43*, 2649–2658. https://doi.org/10.1002/2016GL067720

Fettweis, X., Tedesco, M., van den Broeke, M., & Ettema, J. (2011). Melting trends over the Greenland ice sheet (1958–2009) from spaceborne microwave data and regional climate models. *The Cryosphere*, *5*(2), 359–375. https://doi.org/10.5194/tc-5-359-2011

Forster, R. R., Box, J. E., van den Broeke, M. R., Miège, C., Burgess, E. W., van Angelen, J. H., et al. (2014). Extensive liquid meltwater storage in firn within the Greenland ice sheet. *Nature Geoscience*, *7*(2), 95–98. https://doi.org/10.1038/NGEO2043

Graeter, K. A., Osterberg, E., Ferris, D. G., Hawley, R. L., Marshall, H. P., Lewis, G., et al. (2018). Ice core records of West Greenland melt and climate forcing. *Geophysical Research Letters*, *45*, 3164–3172. https://doi.org/10.1002/2017GL076641

Hanna, E., Huybrechts, P., Steffen, K., Cappelen, J., Huff, R., Shuman, C., et al. (2008). Increased runoff from melt from the Greenland ice sheet: A response to global warming. *Journal of Climate*, *21*(2), 331–341. https://doi.org/10.1175/2007JCLI1964.1

Harper, J., Humphrey, N., Pfeffer, W. T., Brown, J., & Fettweis, X. (2012). Greenland ice-sheet contribution to sea-level rise buffered by meltwater storage in firn. *Nature*, *491*(7423), 240–243. https://doi.org/10.1038/nature11566

Hofer, S., Tedstone, A. J., Fettweis, X., & Bamber, J. L. (2017). Decreasing cloud cover drives the recent mass loss on the Greenland ice sheet. *Science Advances*, *3*(6), e1700584. https://doi.org/10.1126/sciadv.1700584

Janssens, I., & Huybrechts, P. (2000). The treatment of meltwater retention in mass-balance parametrization of the Greenland ice sheet. *Annals of Glaciology*, *31*, 133–140. https://doi.org/10.3189/172756400781819941

Katsushima, T., Kumakura, T., & Takeuchi, Y. (2009). A multiple snow layer model including a parameterization of vertical water channel process in snowpack. *Cold Regions Science and Technology*, *59*(2-3), 143–151. https://doi.org/10.1016/j.coldregions.2009.09.002

Khan, S., Aschwanden, A., Bjork, A., Wahr, J., Kjeldsen, K., & Kjaer, K. (2015). Greenland ice sheet mass balance: A review. *Reports on Progress in Physics*, *78*(4), 046801. https://doi.org/10.1088/0034-4885/78/4/046801

Langen, P., Fausto, R. S., Vandecrux, B., Mottram, R. H., & Box, J. E. (2017). Liquid water flow and retention on the Greenland ice sheet in the regional climate model HIRHAM5: Local and large-scale impacts. *Frontiers in Earth Science*, *4*(110). https://doi.org/10.3389/feart.2016.00110

Langen, P., Mottram, R., Christensen, J., Boberg, F., Rodehacke, C., Stendel, M., et al. (2015). Quantifying energy and mass fluxes controlling Godthåbsfjord freshwater input in a 5-km simulation (1991–2012). *Journal of Climate*, *28*(9), 3694–3713. https://doi.org/10.1175/JCLI-D-14-00271.1

Lefebre, F., Gallée, H., van Ypersele, J., & Greuell, W. (2003). Modelling of snow and ice melt at ETH camp (West Greenland): A study of surface albedo. *Journal of Geophysical Research*, *108*(D8), 4231. https://doi.org/10.1029/2001JD001160

Lomonaco, R., Albert, M., & Baker, I. (2011). Microstructural evolution of fine-grained layers through the firn column at summit, Greenland. *Journal of Glaciology*, *57*(204), 755–762. https://doi.org/10.3189/002214311797409730

Lucas-Picher, P., Wulff-Nielsen, M., Christensen, J. H., Aðalgeirsdóttir, G., Mottram, R., & Simonsen, S. (2012). Very high resolution in regional climate model simulations for Greenland: Identifying added value. *Journal of Geophysical Research*, *117*, D02108. https://doi.org/10.1029/2011JD016267

Machguth, H., MacFerrin, M., van As, D., Box, J. E., Charalampidis, C., Colgan, W., et al. (2016). Greenland meltwater storage in firn limited by near-surface ice formation. *Nature Climate Change*, *6*(4), 390–393. https://doi.org/10.1038/nclimate2899

Marchenko, S., van Pelt, W., Claremar, B., Machguth, H., Reijmer, C., Pettersson, R., & Pohjola, V. (2017). Parameterizing deep water percolation improves subsurface temperature simulations by a multilayer firn model. *Frontiers in Earth Science*, *5*(16). https://doi.org/10.3389/feart.2017.00016

Marsh, P., & Woo, M. (1984). Wetting front advance and freezing of meltwater within a snow cover. 1. Observations in the Canadian Arctic. *Water Resources Research*, *20*(12), 1853–1864. https://doi.org/10.1029/WR020i012p01853

Mayewski, P., & Whitlow, S. (2016). Snow pit data from Greenland summit, 1989 to 1993. *NSF Arctic Data Center*. https://doi.org/10.5065/D6NP22KX

Mosley-Thompson, E., McConnell, J., Bales, R., Li, Z., Lin, P.-N., & Steffen, K. (2001). Local to regional-scale variability of annual net accumulation on the Greenlandice sheet from PARCA cores. *Journal of Glaciology*, *106*(D24), 33,839–33,851. https://doi.org/10.1029/2001JD900067

Mote, T. L. (2007). Greenland surface melt trends 1973–2007: Evidence of a large increase in 2007. *Geophysical Research Letters*, *34*, L22507. https://doi.org/10.1029/2007GL031976

Nghiem, S. V., Hall, D. K., Mote, T. L., Tedesco, M., Albert, M. R., Keegan, K., et al. (2012). The extreme melt across the Greenland ice sheet in 2012. *Geophysical Research Letters*, *39*, L20502. https://doi.org/10.1029/2012GL053611

Orsi, A., Kawamura, K., Masson-Delmotte, V., Fettweis, X., Box, J. E., Dahl-Jensen, D., et al. (2017). The recent warming trend in North Greenland. *Geophysical Research Letters*, *44*, 6235–6243. https://doi.org/10.1002/2016GL072212

Pfeffer, W. T., Meier, M. F., & Illangaskare, T. (1991). Retention of Greenland runoff by refreezing: Implication for projected future sea level change. *Journal of Glaciology*, *96*(C12), 22,117–22,124.

Reijmer, C. H., van den Broeke, M. R., Fettweis, X., Ettema, J., & Stap, L. B. (2012). Refreezing on the Greenland ice sheet: A comparison of parameterizations. *The Cryosphere*, *6*(4), 743–762. https://doi.org/10.5194/tc-6-743-2012

Spencer, M. K., Alley, R. B., & Creyts, T. T. (2001). Preliminary firn-densification model with 38-site dataset. *Journal of Glaciology*, *96*(C12), 671–676. https://doi.org/10.1029/91JC02502

Steffen, K., & Box, J. E. (2001). Surface climatology of the Greenland ice sheet: Greenland climate network 1995–1999. *Journal of Glaciology*, *106*(D24), 33,951–33,964. https://doi.org/10.1029/2001JD900161

Steffen, K., Box, J. E., & Abdalati, W. (1996). Greenland climate network: GC-net. In S. C. Colbeck (Ed.), *Special Report on Glaciers, Ice Sheets and Volcanoes, trib. to M. Meier*, (pp. 98–103). CRREL 96–27. Hanover, NH.

Steger, C. R., Reijmer, C. H., & van den Broeke, M. R. (2017). The modelled liquid water balance of the Greenland ice sheet. *The Cryosphere*, *11*(6), 2507–2526. https://doi.org/10.5194/tc-11-2507-2017

Tardivo, G., & Berti, A. (2012). A dynamic method for gap filling in daily temperature datasets. *Journal of Applied Meteorology*, *51*(6), 1079–1086. https://doi.org/10.1175/JAMC-D-11-0117.1

Tedesco, M., Fettweis, X., van den Broeke, M. R., van de Wal, R. S., Smeets, C. J., van de Berg, W. J., et al. (2011). The role of albedo and accumulation in the 2010 melting record in Greenland. *Environmental Research Letters*, *6*(1). https://doi.org/10.1088/1748-9326/6/1/014005

van Angelen, J. H., Lenaerts, J., van den Broeke, M. R., Fettweis, X., & van Meijgaard, E. (2013). Rapid loss of firn pore space accelerates 21st century Greenland mass loss. *Geophysical Research Letters*, *40*, 2109–2113. https://doi.org/10.1002/grl.50490

van As, D., Hubbard, A. L., Hasholt, B., Mikkelsen, A. B., van den Broeke, M. R., & Fausto, R. S. (2012). Large surface meltwater discharge from the Kangerlussuaq sector of the Greenland ice sheet during the record-warm year 2010 explained by detailed energy balance observations. *The Cryosphere*, *6*(1), 199–209. https://doi.org/10.5194/tc-6-199-2012

van As, D., Mikkelsen, A. B., Nielsen, M. H., Box, J. E., Liljedahl, L. C., Lindbäck, K., et al. (2017). Hypsometric amplification and routing moderation of Greenland ice sheet meltwater release. *The Cryosphere*, *11*(3), 1371–1386. https://doi.org/10.5194/tc-11-1371-2017

van As, D., van den Broeke, M., Reijmer, C., & van de Wal, R. (2005). The summer surface energy balance of the high Antartic plateau. *Boundary-Layer Meteorology*, *115*(2), 289–317. https://doi.org/10.1007/s10546-004-4631-1

van den Broeke, M. R., Enderlin, E. M., Howat, I. M., Kuipers Munneke, P., Noël, B. P., van de Berg, W. J., et al. (2016). On the recent contribution of the Greenland ice sheet to sea level change. *The Cryosphere*, *10*(5), 1933–1946. https://doi.org/10.5194/tc-10-1933-2016

van Tricht, K., Lhermitte, S., Lenaerts, J. T., Gorodetskaya, I. V., L'Ecuyer, T. S., Noël, B., et al. (2016). Clouds enhance Greenland ice sheet meltwater runoff. *Nature Communications*, *7*, 10266. https://doi.org/10.1038/ncomms10266

Vionnet, V., Brun, E. S., Eisen, A., Fierz, C., & Lehning, M. (2012). The detailed snowpack scheme Crocus and its implementation in SURFEXv7.2. *Geoscientific Model Development*, *5*(3), 773–791. https://doi.org/10.5194/gmd-5-773-2012

Wever, N., Fierz, C., Mitterer, C., Hirashima, H., & Lehning, M. (2014). Solving Richards equation for snow improves snowpack meltwater runoff estimations in detailed multi-layer snowpack model. *The Cryosphere*, *8*(1), 257–274. https://doi.org/10.5194/tc-8-257-2014

Wever, N., Würzer, S., Fierz, C., & Lehning, M. (2016). Simulating ice layer formation under the presence of preferential flow in layered snowpacks. *The Cryosphere*, *10*(6), 2731–2744. https://doi.org/10.5194/tc-10-2731-2016

Yen, Y. (1981). *Review of Thermal Properties of Snow, Ice and Sea Ice*. Hanover,NH: United States Army Cold Regions Research and Engineering Laboratory.